

## SUPPLEMENTARY INFORMATION

### **Interpreting Tafel Behavior of Consecutive Electrochemical Reactions through Combined Thermodynamic and Steady State Microkinetic Approaches**

J. Tyler Mefford,<sup>1,2,†,\*</sup> Zhenghang Zhao,<sup>3,‡,§</sup> Michal Bajdich,<sup>3,\*</sup> William C. Chueh<sup>1,2</sup>

<sup>1</sup>Department of Materials Science and Engineering, Stanford University, Stanford, CA 94305. <sup>2</sup>Stanford Institute for Materials and Energy Sciences, SLAC National Accelerator Laboratory, Menlo Park, CA 94025. <sup>3</sup> SUNCAT Center for Interface Science and Catalysis, Department of Chemical Engineering, Stanford University, Stanford, CA 94305.

## Quasi-equilibrium microkinetic modeling of the Oxygen Evolution Reaction on $\text{CoO}_x(\text{OH})_{2-x}$ :

In the quasi-equilibrium approach, the net reaction is modeled through an *a priori* assumption about which elementary reaction is the RLS.<sup>1</sup> Each reaction step is modeled as a possible rate-limiting step resulting in 4 different fits of the data for a given bulk phase and surface condition, one for each possible rate-limiting step. The quasi-equilibrium approach assumes that reactions that *precede* the rate-limiting step are in equilibrium, i.e. their intrinsic exchange rates are significantly faster than the RLS such that the adsorbate concentrations are governed solely by the thermodynamics of the system. In addition, the coverage of the reactant of the RLS is assumed to build-up in the forward direction of the reaction such that it approaches monolayer coverage and reactions that *follow* the RLS are ignored as contributing to the RLS with their coverages approaching zero.<sup>1-3</sup> Only the forward rate of the rate-limiting step is considered, and the product adsorbate is ignored in contributing to the coverage. The goodness of fit is measured through the RMS log error in order to isolate the RLS that fits the data the best.

Similar to the steady state approach, the kinetics of the reaction are evaluated through the Butler-Volmer framework:

$$\bar{k}_i = k_i^0 e^{[(1-\beta_i)f(E-E_{i,DFT}^0)]} \quad (\text{S1})$$

$$\tilde{k}_i = k_i^0 e^{[-\beta_i f(E-E_{i,DFT}^0)]} \quad (\text{S2})$$

$$v_i = \bar{k}_i \theta_{i,R} - \tilde{k}_i \theta_{i,P} \quad (\text{S3})$$

The quasi-equilibrium approximation assumes a single RLS, where the rate of this elementary reaction,  $v_{RLS}$ , governs the overall current density,  $j_{model}$ , according to:

$$j_{model} = 4F\Gamma_{geom}v_{RLS} \quad (\text{S4})$$

Reactions that precede the RLS are assumed to be in equilibrium such that the forward and backward rates are equal making equation [S3] sum to zero and allowing for the coverage of the given adsorbates to be determined:

$$\frac{\vec{k}_i\theta_{i,R}}{\vec{k}_i\theta_{i,P}} = 1 \quad (S5)$$

For the RLS reaction only the forward reaction rate is considered:

$$v_{RLS} = \vec{k}_{i,RLS}\theta_{i,R,RLS} \quad (S6)$$

In addition, the coverage (which considers only the adsorbates preceding and involved in the RLS) is assumed to follow Langmuir adsorption assumptions and saturate at a single monolayer:

$$\sum_{i=1}^{RLS} \theta_i = 1 \quad (S7)$$

With these constraints in mind, we can evaluate the functional form of the rate and voltage dependent coverage for each of the possible rate-limiting steps, where the net reaction rate equations are given in the main text equations (9-12).

If reaction (1) is the RLS, the adsorbate coverages and rate of the RLS are:

$$\theta_* = 1 \quad (S8)$$

$$v_1 = v_{RLS} = \vec{k}_1\theta_* = k_1^0\theta_*e^{[(1-\beta_1)f(E-E_{1,DFT}^0)]} \quad (S9)$$

If reaction (2) is the RLS, the adsorbate coverages and rate of the RLS are:

$$\theta_* = 1 - \theta_{OH} \quad (S10)$$

$$\theta_{OH} = \frac{e^{f(E-E_{1,DFT}^0)}}{1+e^{f(E-E_{1,DFT}^0)}} \quad (S11)$$

$$v_2 = v_{RLS} = \vec{k}_2\theta_{OH} = k_2^0\theta_{OH}e^{[(1-\beta_2)f(E-E_{2,DFT}^0)]} \quad (S12)$$

If reaction (3) is the RLS, the adsorbate coverages and rate of the RLS are:

$$\theta_* = 1 - \theta_{OH} - \theta_O \quad (S13)$$

$$\theta_{OH} = \frac{e^{f(E-E_{1,DFT}^{0'})}}{1+e^{f(E-E_{1,DFT}^{0'})}+e^{f(2E-E_{1,DFT}^{0'}-E_{2,DFT}^{0'})}} \quad (S14)$$

$$\theta_O = \frac{e^{f(2E-E_{1,DFT}^{0'}-E_{2,DFT}^{0'})}}{1+e^{f(E-E_{1,DFT}^{0'})}+e^{f(2E-E_{1,DFT}^{0'}-E_{2,DFT}^{0'})}} \quad (S15)$$

$$v_3 = v_{RLS} = \vec{k}_3 \theta_O = k_3^0 \theta_O e^{[(1-\beta_3)f(E-E_{3,DFT}^{0'})]} \quad (S16)$$

If reaction (4) is the RLS, the adsorbate coverages and rate of the RLS are:

$$\theta_* = 1 - \theta_{OH} - \theta_O - \theta_{OOH} \quad (S17)$$

$$\theta_{OH} = \frac{e^{f(E-E_{1,DFT}^{0'})}}{1+e^{f(E-E_{1,DFT}^{0'})}+e^{f(2E-E_{1,DFT}^{0'}-E_{2,DFT}^{0'})}+e^{f(3E-E_{1,DFT}^{0'}-E_{2,DFT}^{0'}-E_{3,DFT}^{0'})}} \quad (S18)$$

$$\theta_O = \frac{e^{f(2E-E_{1,DFT}^{0'}-E_{2,DFT}^{0'})}}{1+e^{f(E-E_{1,DFT}^{0'})}+e^{f(2E-E_{1,DFT}^{0'}-E_{2,DFT}^{0'})}+e^{f(3E-E_{1,DFT}^{0'}-E_{2,DFT}^{0'}-E_{3,DFT}^{0'})}} \quad (S19)$$

$$\theta_{OOH} = \frac{e^{f(3E-E_{1,DFT}^{0'}-E_{2,DFT}^{0'}-E_{3,DFT}^{0'})}}{1+e^{f(E-E_{1,DFT}^{0'})}+e^{f(2E-E_{1,DFT}^{0'}-E_{2,DFT}^{0'})}+e^{f(3E-E_{1,DFT}^{0'}-E_{2,DFT}^{0'}-E_{3,DFT}^{0'})}} \quad (S20)$$

$$v_4 = v_{RLS} = \vec{k}_4 \theta_{OOH} = k_4^0 \theta_{OOH} e^{[(1-\beta_4)f(E-E_{4,DFT}^{0'})]} \quad (S21)$$

The results of the quasi-equilibrium microkinetic model fits for the DFT self-consistent conditions are presented in Figure S2 and the standard rate constants and symmetry coefficient with their 95% confidence intervals and RMS log error presented in Table S1. The results of the quasi-equilibrium microkinetic model fits for the other considered surfaces and coverage conditions are included in Figure S3 and Table S2 in the Supplementary Information. A description of the confidence interval calculations is included below. We note that the rationale behind selecting the three coverage

scenarios presented in Figure S2 as follow from the DFT self-consistent conditions evaluated through the steady state portion of this work.

In general, the fits of the microkinetic modelling using the quasi-equilibrium approach are poor with large RMS Log errors and symmetry coefficients approaching unreasonable extremes of  $\beta \rightarrow 1$ . The best fits are generally for a RLS of  $* \rightarrow \text{OH}^*$  or  $\text{OH}^* \rightarrow \text{O}^*$  on all surfaces.

Similar to the improved steady state approach, a bulk phase change reaction can be incorporated into the quasi-equilibrium model as well, as described through equations (22-25) and Figure 6 of the main text. The fitting results of the quasi-equilibrium microkinetic model including the “phase-change” reaction for the DFT self-consistent conditions are presented in Figure S4 and the standard rate constants, symmetry coefficients, and standard phase change voltage with their 95% confidence intervals and RMS log error presented in Table S3. The fitting results of the quasi-equilibrium microkinetic model including the phase-change reaction for the other considered surfaces and coverage conditions are included in Figure S5 and Table S4.

By considering the concentration of active species at the surface as a function of applied voltage, the microkinetic model can now fit the data well for certain rate-limiting steps on the  $\text{CoO}_x(\text{OH})_{2-x}$  surfaces. Still, the fit is poor for the  $\beta\text{-Co}(\text{OH})_2$  surface which is reasonable as this is not likely to be the active OER species, i.e. at open-circuit conditions where  $\beta\text{-Co}(\text{OH})_2$  is assumed to be the bulk phase there is no spontaneous evolution of oxygen. Only a RLS of  $\text{O}^* \rightarrow \text{OOH}^*$  on the  $\beta\text{-Co}(\text{OH})_2$  surface fits the data well, but examination of the high voltage data suggests decreasing current density with increasing overpotential which is inconsistent with experiment. Examining the results of the microkinetic model fits for the other  $\text{CoO}_x(\text{OH})_{2-x}$  phases, the model predicts the RLS well. However, for reactions that are not the RLS,  $E^0_{\text{PhaseChange}}$  falls outside of the bounds of the experimental data ( $< 1.5\text{V}$  vs. RHE or  $> 1.9\text{V}$  vs. RHE) resulting in the same fits as for the quasi-equilibrium model without considering the phase

change reaction, implying that including this extra degree of freedom does not improve the fit. In addition, this approach is not able to differentiate between which RLS, either  $* \rightarrow \text{OH}^*$  or  $\text{OH}^* \rightarrow \text{O}^*$ , is operative on the  $\beta\text{-CoOOH}$  or  $\text{CoO}_2$  ( $11\bar{2}0$ ) surfaces as the model provides equally suitable fits. This result is reminiscent of the “dual reaction barrier” previously been suggested by Lyons and Brandon for the OER on Co anodes.<sup>4</sup> In addition Bergmann *et al.* have reported the presence of four and five fold coordinated cobalt ions during the OER on  $\beta\text{-CoOOH}$  suggestive of empty terminal surface sites on the ( $11\bar{2}0$ ) surface which is in agreement with the results of the microkinetic modeling for the DFT considered surfaces and RLS's of either  $* \rightarrow \text{OH}^*$  or  $\text{OH}^* \rightarrow \text{O}^*$ .<sup>5,6</sup> For the determined rate-limiting steps, the symmetry coefficient was close to 0.5 for all surfaces considered which demonstrates the ability of the model to describe the kinetics of the system within a reasonable energetic framework. We note that while symmetry coefficients much different than 0.5 have been used to describe OER kinetics, in general electron transfer tends to have symmetric or very close to symmetric barriers corresponding to  $\beta = 0.5$ .<sup>7,8</sup> For the determined rate-limiting steps, the calculated redox phase-change standard voltage was determined to be between 1.562-1.593V vs. RHE which corresponds well to the previously observed high voltage redox peak.<sup>9</sup> We believe that the primary inadequacy of differentiating rate-limiting steps for given surface coverage conditions using the quasi-equilibrium approach derives from its assumptions on contributions of reactions following the forward direction of the rate-limiting step. This assumption ignores any contributions of concentration overpotentials can arise if the potential is below the thermodynamic potential for a given reaction (i.e. back reaction contributes) or the kinetics for a given step have minor but significant contributions. As such, we do not believe the quasi-equilibrium approach is a valid approximation for evaluation the reaction kinetics of consecutive electrochemical reactions. A better approach which improves upon the assumptions of the quasi-equilibrium approach is the steady state approach which is described in the main text.

## Solutions to the Steady State Adsorbate Coverage as a Function of Voltage:

The solutions to the system of equations (equations 9-16 of the main text) that describe the steady state adsorbate coverage as a function of voltage are:

$$\theta_* = \frac{\bar{k}_1 \bar{k}_3 \bar{k}_4 + \bar{k}_2 \bar{k}_3 \bar{k}_4 + \bar{k}_1 \bar{k}_2 \bar{k}_3 + \bar{k}_1 \bar{k}_2 \bar{k}_4}{\bar{k}_1 \bar{k}_3 \bar{k}_4 + \bar{k}_2 \bar{k}_3 \bar{k}_4 + \bar{k}_2 \bar{k}_3 \bar{k}_1 + \bar{k}_3 \bar{k}_4 \bar{k}_2 + \bar{k}_3 \bar{k}_1 \bar{k}_2 + \bar{k}_4 \bar{k}_2 \bar{k}_3 + \bar{k}_1 \bar{k}_2 \bar{k}_3 + \bar{k}_2 \bar{k}_1 \bar{k}_4 + \bar{k}_1 \bar{k}_2 \bar{k}_4 + \bar{k}_1 \bar{k}_3 \bar{k}_4 + \bar{k}_2 \bar{k}_3 \bar{k}_4 + \bar{k}_1 \bar{k}_3 \bar{k}_4 + \bar{k}_1 \bar{k}_3 \bar{k}_4 + \bar{k}_1 \bar{k}_2 (\bar{k}_3 + \bar{k}_4 + \bar{k}_4)} \quad (S22)$$

$$\theta_{OH} = \frac{\bar{k}_1 \theta_* + \bar{k}_2 \theta_O}{\bar{k}_1 + \bar{k}_2} \quad (S23)$$

$$\theta_O = \frac{\bar{k}_1 \bar{k}_2 \theta_* + \bar{k}_1 \bar{k}_3 \theta_{OOH} + \bar{k}_3 \bar{k}_2 \theta_{OOH}}{\bar{k}_1 \bar{k}_2 + \bar{k}_1 \bar{k}_3 + \bar{k}_2 \bar{k}_3} \quad (S24)$$

$$\theta_{OOH} = \frac{(\bar{k}_4 \bar{k}_2 \bar{k}_3 + \bar{k}_1 \bar{k}_2 \bar{k}_3 + \bar{k}_1 \bar{k}_2 \bar{k}_4 + \bar{k}_1 \bar{k}_4 \bar{k}_3) \theta_*}{\bar{k}_1 \bar{k}_3 \bar{k}_4 + \bar{k}_2 \bar{k}_3 \bar{k}_4 + \bar{k}_1 \bar{k}_2 \bar{k}_3 + \bar{k}_1 \bar{k}_2 \bar{k}_4} \quad (S25)$$

## Confidence Intervals for Derived Rate Constants in the Quasi-equilibrium Model<sup>10</sup>

The rate constants,  $k_{1-4}^0$ , and the symmetry coefficients,  $\beta_{1-4}$  were used as the fitting parameters for the microkinetic model described in the main text for each possible rate-limiting step, Equations [14, 17, 21, 26]. The model was fit to 219 data points yielding a degree of freedom ( $\nu$ ) of 217. The confidence interval is described as, where  $k_i^0$  is the standard rate constant for elementary reaction  $i$ ,  $t$  is the value of the student's t-distribution with 217 degrees of freedom and a 95% confidence interval, and  $\text{diag}$  is an operator that takes the diagonal of the matrix  $\sqrt{S}$ :

$$k_i^0 \pm t_{\alpha=0.025, \nu=217} \text{diag}(\sqrt{S}) \quad (S26)$$

The covariance matrix,  $S$ , is defined as:

$$S = R^2 (A^T A)^{-1} \quad (S27)$$

Where  $A$  is the Jacobian matrix of the fitted values with regards to the fitted coefficients,  $A^T$  is the transpose matrix of  $A$ , and  $R^2$  is the mean square log error:

$$R^2 = \frac{1}{\nu} \sum (\log j_{exp} - \log j_{model})^2 \quad (S28)$$

The Jacobian matrix  $A$  is the partial derivative matrix of  $j$  with respect to the rate constants, i.e.:

$$A = \begin{bmatrix} \frac{\partial j_1}{\partial k_i} & \frac{\partial j_1}{\partial \beta_i} \\ \frac{\partial j_2}{\partial k_i} & \frac{\partial j_2}{\partial \beta_i} \\ \vdots & \vdots \\ \frac{\partial j_{219}}{\partial k_i} & \frac{\partial j_{219}}{\partial \beta_i} \end{bmatrix} \quad (S29)$$

### Confidence Intervals for Derived Rate Constants in the Quasi-equilibrium with Phase-Change Reaction Model<sup>10</sup>

The confidence interval was calculated in a similar manner as for the quasi-equilibrium model without the phase-change reaction, but in this case an additional parameter,  $E_{PhaseChange}^0$  (Equations [27, 30] from the main text, shown in the Jacobian matrix as  $E_{PC}$ ), was included resulting in a degrees of freedom of  $\nu = 216$  and a Jacobian matrix  $A$  of:

$$A = \begin{bmatrix} \frac{\partial j_1}{\partial k_i} & \frac{\partial j_1}{\partial \beta_i} & \frac{\partial j_1}{\partial E_{PC,i}} \\ \frac{\partial j_2}{\partial k_i} & \frac{\partial j_2}{\partial \beta_i} & \frac{\partial j_2}{\partial E_{PC,i}} \\ \vdots & \vdots & \vdots \\ \frac{\partial j_{219}}{\partial k_i} & \frac{\partial j_{219}}{\partial \beta_i} & \frac{\partial j_{219}}{\partial E_{PC,i}} \end{bmatrix} \quad (S30)$$

### Confidence Intervals for Derived Rate Constants in the Steady State Model<sup>10</sup>

The confidence interval was calculated in a similar manner to the above quasi-equilibrium cases, but in this situation there are four fitting parameters, the rate constants,  $k_{1-4}^0$ , which are used to fit Equations [7, 8, 31-34] of the main text, yielding a degree of freedom ( $\nu$ ) of 215, and a Jacobian matrix  $A$ :

$$A = \begin{bmatrix} \frac{\partial j_1}{\partial k_1^0} & \frac{\partial j_1}{\partial k_2^0} & \frac{\partial j_1}{\partial k_3^0} & \frac{\partial j_1}{\partial k_4^0} \\ \frac{\partial j_2}{\partial k_1^0} & \frac{\partial j_2}{\partial k_2^0} & \frac{\partial j_2}{\partial k_3^0} & \frac{\partial j_2}{\partial k_4^0} \\ \vdots & \vdots & \vdots & \vdots \\ \frac{\partial j_{219}}{\partial k_1^0} & \frac{\partial j_{219}}{\partial k_2^0} & \frac{\partial j_{219}}{\partial k_3^0} & \frac{\partial j_{219}}{\partial k_4^0} \end{bmatrix} \quad (S31)$$

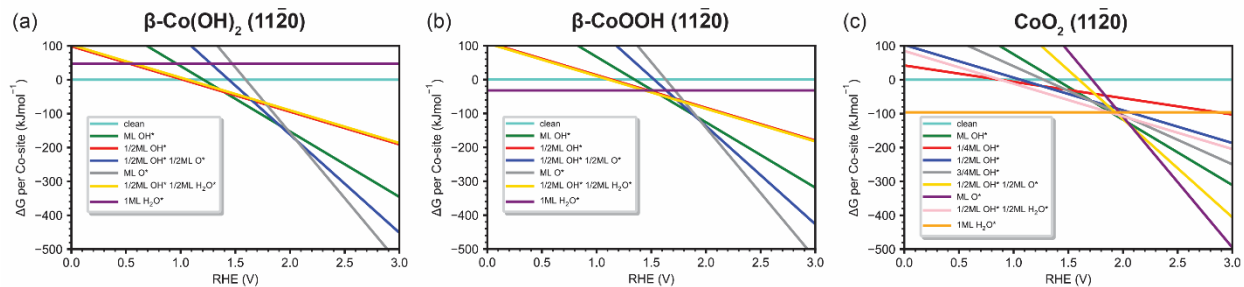


**Figure S1. Free energies of surface coverages as a function of voltage for the  $\text{CoO}_x(\text{OH})_{2-x}$  ( $11\bar{2}0$ ) surfaces. Coverage of 1ML corresponds to two adsorbed species per Co surface atom.**

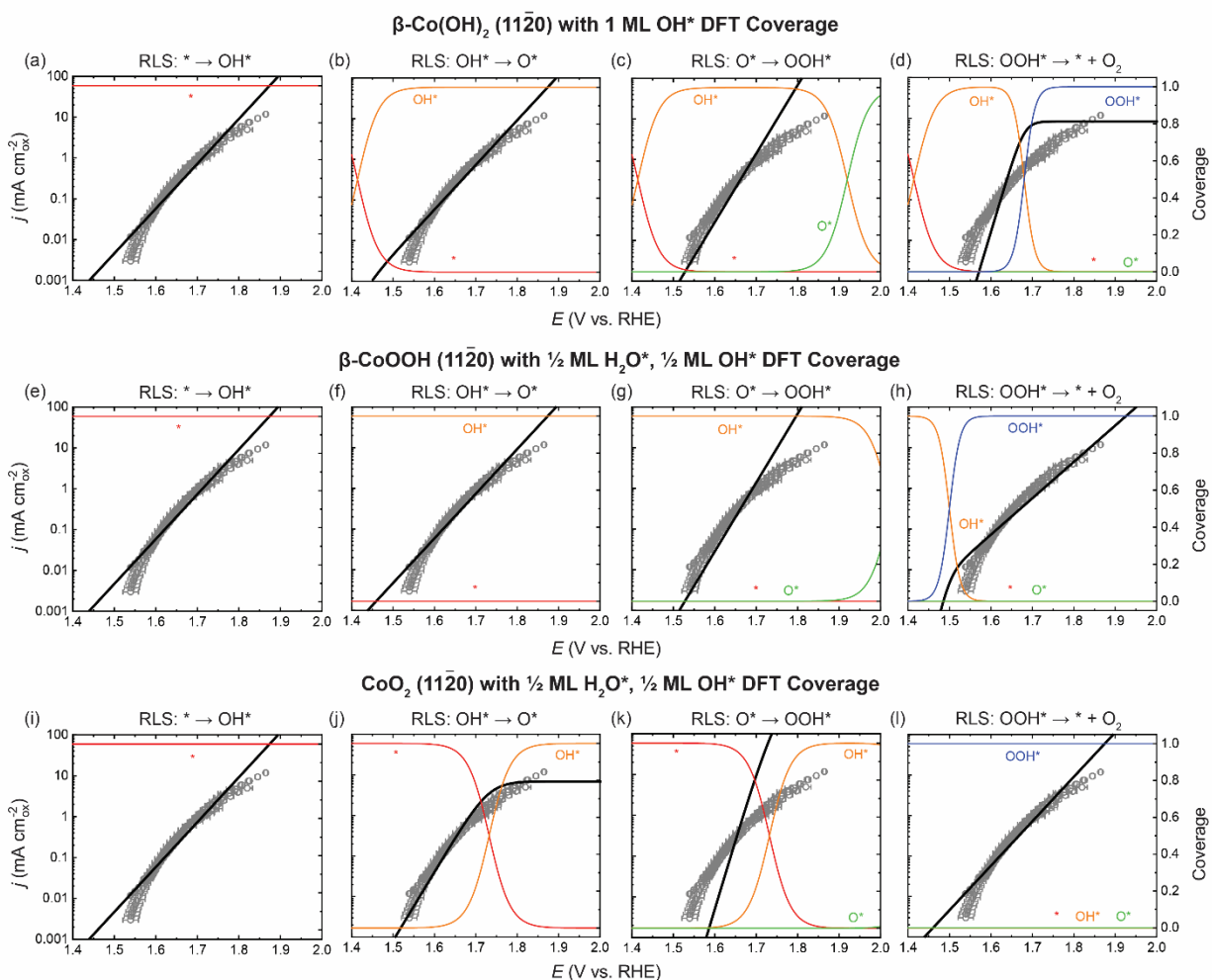


**Figure S2. Quasi-equilibrium microkinetic fits for the DFT self-consistent  $\text{CoO}_x(\text{OH})_{2-x}$  ( $11\bar{2}0$ ) surfaces.** The fits are shown in black and the coverage predicted by the quasi-equilibrium microkinetic model shown in red for the clean surface, orange for  $\text{OH}^*$ , green for  $\text{O}^*$ , and blue for  $\text{OOH}^*$  for the (a-d)  $\beta\text{-Co}(\text{OH})_2$  ( $11\bar{2}0$ ) surface with 1 ML  $\text{OH}^*$  DFT coverage, (e-h)  $\beta\text{-CoOOH}$  ( $11\bar{2}0$ ) surface with  $\frac{1}{2}$  ML  $\text{H}_2\text{O}^*$ ,  $\frac{1}{2}$  ML  $\text{OH}^*$  DFT coverage, and (i-l) the  $\text{CoO}_2$  ( $11\bar{2}0$ ) surface with  $\frac{1}{2}$  ML  $\text{H}_2\text{O}^*$ ,  $\frac{1}{2}$  ML  $\text{OH}^*$  DFT coverage. For (a,e,i) the RLS was assumed to be Reaction 1,  $* \rightarrow \text{OH}^*$ , (b,f,j) the RLS was assumed to be Reaction 2,  $\text{OH}^* \rightarrow \text{O}^*$ , (c,g,k) the RLS was assumed to be Reaction 3,  $\text{O}^* \rightarrow \text{OOH}^*$ , and for (d,h,l) the RLS was assumed to be Reaction 4,  $\text{OOH}^* \rightarrow * + \text{O}_2$ .

**Table S1: Quasi-equilibrium microkinetic modeling standard rate constants,  $k_i^0$ , symmetry coefficients,  $\beta_i$ , with 95% Confidence Intervals and RMS Log Error for fits of each possible rate limiting step on the DFT self-consistent  $\text{CoO}_x(\text{OH})_{2-x}$  ( $11\bar{2}0$ ) surfaces.**

Phase:	DFT Coverage Conditions:	RLS	$k_i^0$ ( $\text{s}^{-1}$ )	$\beta_i$	RMS Log Error
$\beta\text{-Co}(\text{OH})_2$	1 ML $\text{OH}^*$	$* \rightarrow \text{OH}^*$	$(2.1 \pm 0.3) \times 10^{-3}$	$0.35 \pm 0.02$	2.40
		$\text{OH}^* \rightarrow \text{O}^*$	$(8 \pm 1) \times 10^2$	$0.35 \pm 0.02$	2.40
		$\text{O}^* \rightarrow \text{OOH}^*$	$(3 \pm 1) \times 10^4$	$1.00 \pm 0.05$	6.51
		$\text{OOH}^* \rightarrow * + \text{O}_2$	$30 \pm 100$	$1.00 \pm 0.07$	10.9
$\beta\text{-CoOOH}$	$\frac{1}{2}$ ML $\text{H}_2\text{O}^*$	$* \rightarrow \text{OH}^*$	$(1.4 \pm 0.4) \times 10^{-6}$	$0.35 \pm 0.02$	2.40
	$\frac{1}{2}$ ML $\text{OH}^*$	$\text{OH}^* \rightarrow \text{O}^*$	$22 \pm 8$	$1.00 \pm 0.02$	2.88
		$\text{O}^* \rightarrow \text{OOH}^*$	$(1 \pm 2) \times 10^6$	$1.00 \pm 0.05$	6.54
		$\text{OOH}^* \rightarrow * + \text{O}_2$	$(1.3 \pm 0.7) \times 10^8$	$0.47 \pm 0.02$	3.18
$\text{CoO}_2$	$\frac{1}{2}$ ML $\text{H}_2\text{O}^*$	$* \rightarrow \text{OH}^*$	$5.3 \pm 0.4$	$0.35 \pm 0.01$	2.40
		$\text{OH}^* \rightarrow \text{O}^*$	$(2.0 \pm 0.6) \times 10^5$	$0.39 \pm 0.01$	1.72
	$\frac{1}{2}$ ML $\text{OH}^*$	$\text{O}^* \rightarrow \text{OOH}^*$	$(2 \pm 20) \times 10^9$	$1.0 \pm 0.2$	19.6
		$\text{OOH}^* \rightarrow * + \text{O}_2$	$(8 \pm 3) \times 10^{-8}$	$0.35 \pm 0.02$	2.41

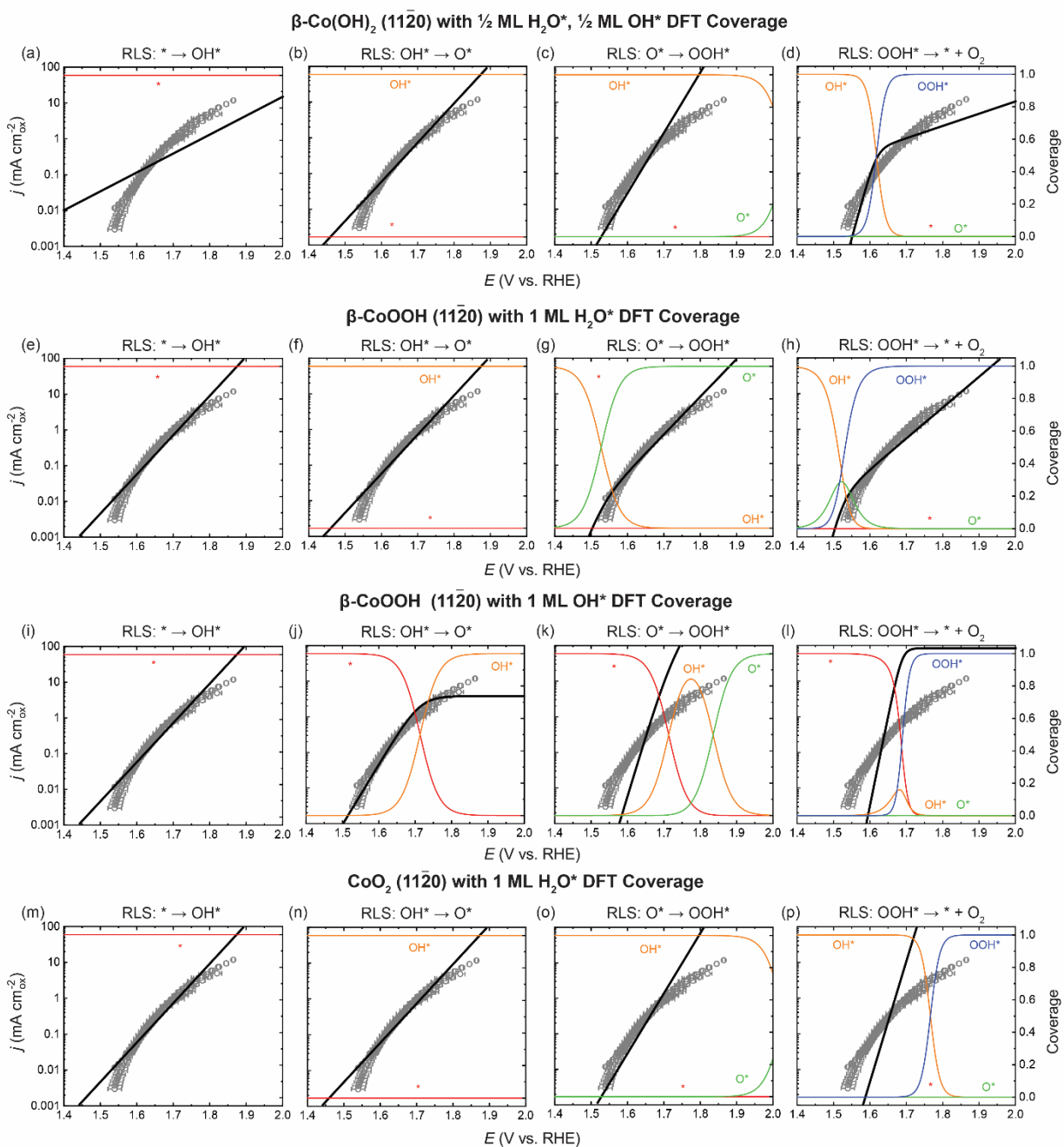


**Figure S3. Quasi-equilibrium microkinetic fits for the DFT non-self-consistent  $\text{CoO}_x(\text{OH})_{2-x}$  ( $11\bar{2}0$ ) surfaces.** The fits are shown in black and the coverage predicted by the quasi-equilibrium microkinetic model shown in red for the clean surface, orange for  $\text{OH}^*$ , green for  $\text{O}^*$ , and blue for  $\text{OOH}^*$  for the (a-d)  $\beta\text{-Co}(\text{OH})_2$  ( $11\bar{2}0$ ) surface with  $\frac{1}{2}$  ML  $\text{H}_2\text{O}^*$ ,  $\frac{1}{2}$  ML  $\text{OH}^*$  DFT coverage, (e-h)  $\beta\text{-CoOOH}$  ( $11\bar{2}0$ ) surface with 1 ML  $\text{H}_2\text{O}^*$  DFT coverage, (i-l)  $\beta\text{-CoOOH}$  ( $11\bar{2}0$ ) surface with 1 ML  $\text{OH}^*$  DFT coverage, and (m-p) the  $\text{CoO}_2$  ( $11\bar{2}0$ ) surface with 1 ML  $\text{H}_2\text{O}^*$  DFT coverage. For (a,e,i,m) the RLS was assumed to be Reaction 1,  $* \rightarrow \text{OH}^*$ , (b,f,j,n) the RLS was assumed to be Reaction 2,  $\text{OH}^* \rightarrow \text{O}^*$ , (c,g,k,o) the RLS was assumed to be Reaction 3,  $\text{O}^* \rightarrow \text{OOH}^*$ , and for (d,h,l,p) the RLS was assumed to be Reaction 4,  $\text{OOH}^* \rightarrow * + \text{O}_2$ .

**Table S2: Quasi-equilibrium microkinetic modeling standard rate constants,  $k_i^0$ , symmetry coefficients,  $\beta_i$ , with 95% Confidence Intervals and RMS Log Error for fits of each possible rate limiting step on the DFT non-self-consistent  $\text{CoO}_x(\text{OH})_{2-x}$  (11 $\bar{2}$ 0) surfaces.**

Phase:	DFT Coverage Conditions:	RLS	$k_i^0$ (s <sup>-1</sup> )	$\beta_i$	RMS Log Error
$\beta\text{-Co}(\text{OH})_2$	$\frac{1}{2}$ ML $\text{H}_2\text{O}^*$ $\frac{1}{2}$ ML $\text{OH}^*$	$* \rightarrow \text{OH}^*$	$(4 \pm 23) \times 10^{-9}$	$0.69 \pm 0.05$	6.34
		$\text{OH}^* \rightarrow \text{O}^*$	$(1.4 \pm 0.3) \times 10^4$	$0.35 \pm 0.02$	2.40
		$\text{O}^* \rightarrow \text{OOH}^*$	$(3 \pm 2) \times 10^6$	$1.00 \pm 0.05$	6.54
		$\text{OOH}^* \rightarrow * + \text{O}_2$	$2.0 \pm 0.2$	$0.80 \pm 0.03$	4.99
$\beta\text{-CoOOH}$	1 ML $\text{H}_2\text{O}^*$	$* \rightarrow \text{OH}^*$	$(1.1 \pm 0.4) \times 10^{-6}$	$0.35 \pm 0.02$	2.40
		$\text{OH}^* \rightarrow \text{O}^*$	$(3.1 \pm 0.3) \times 10^{-2}$	$0.35 \pm 0.02$	2.40
		$\text{O}^* \rightarrow \text{OOH}^*$	$(2.8 \pm 0.3) \times 10^{-2}$	$0.38 \pm 0.02$	2.03
		$\text{OOH}^* \rightarrow * + \text{O}_2$	$(1.2 \pm 0.7) \times 10^{-8}$	$0.49 \pm 0.2$	2.92
$\beta\text{-CoOOH}$	1 ML $\text{OH}^*$	$* \rightarrow \text{OH}^*$	$3.4 \pm 0.2$	$0.35 \pm 0.02$	2.41
		$\text{OH}^* \rightarrow \text{O}^*$	$13 \pm 1$	$1.00 \pm 0.01$	2.24
		$\text{O}^* \rightarrow \text{OOH}^*$	$(2 \pm 1) \times 10^4$	$1.0 \pm 0.1$	18.0
		$\text{OOH}^* \rightarrow * + \text{O}_2$	$(3 \pm 30) \times 10^2$	$1.0 \pm 0.2$	23.1
$\text{CoO}_2$	1 ML $\text{H}_2\text{O}^*$	$* \rightarrow \text{OH}^*$	$(1.3 \pm 0.5) \times 10^{-7}$	$0.35 \pm 0.02$	2.40
		$\text{OH}^* \rightarrow \text{O}^*$	$(1.0 \pm 0.2) \times 10^4$	$0.35 \pm 0.02$	2.40
		$\text{O}^* \rightarrow \text{OOH}^*$	$(1.7 \pm 0.6) \times 10^6$	$1.00 \pm 0.05$	6.54
		$\text{OOH}^* \rightarrow * + \text{O}_2$	$(6 \pm 40) \times 10^4$	$1.0 \pm 0.1$	20.4

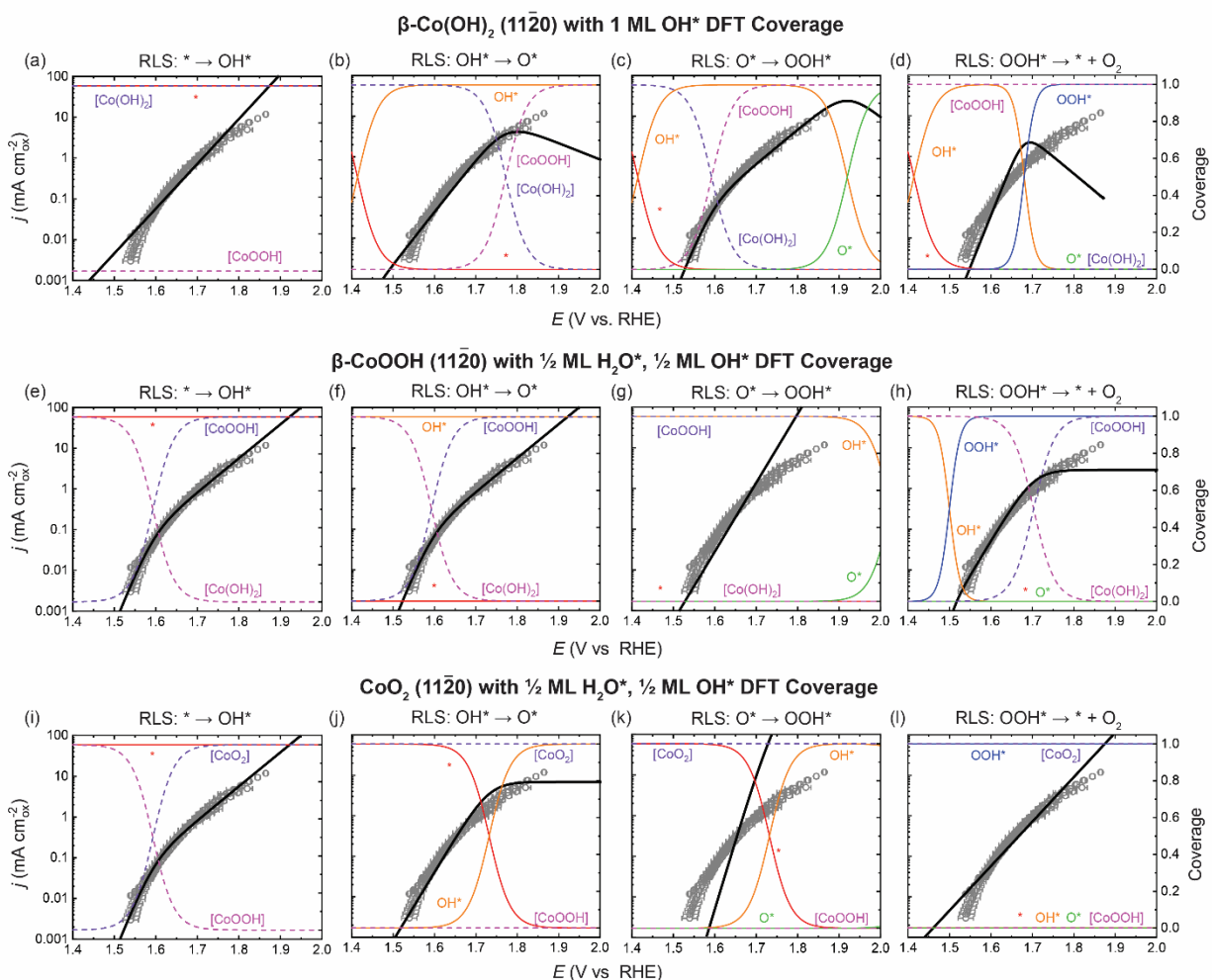


**Figure S4. Quasi-equilibrium with phase-change reaction microkinetic fits for the DFT self-consistent  $\text{CoO}_x(\text{OH})_{2-x}$  ( $11\bar{2}0$ ) surfaces.** The fits are shown in black and the coverage predicted by the quasi-equilibrium microkinetic model shown in red for the clean surface, orange for  $\text{OH}^*$ , green for  $\text{O}^*$ , and blue for  $\text{OOH}^*$ , purple for the active phase, and magenta for the inactive phase for the (a-d)  $\beta\text{-Co(OH)}_2$  ( $11\bar{2}0$ ) surface with 1 ML  $\text{OH}^*$  DFT coverage, (e-h)  $\beta\text{-CoOOH}$  ( $11\bar{2}0$ ) surface with  $\frac{1}{2}$  ML  $\text{H}_2\text{O}^*$ ,  $\frac{1}{2}$  ML  $\text{OH}^*$  DFT coverage, and (i-l) the  $\text{CoO}_2$  ( $11\bar{2}0$ ) surface with  $\frac{1}{2}$  ML  $\text{H}_2\text{O}^*$ ,  $\frac{1}{2}$  ML  $\text{OH}^*$  DFT coverage. We note that the calculated adsorbate coverages correspond to the coverage only on the active phase. For (a,e,i) the RLS was assumed to be Reaction 1,  $* \rightarrow \text{OH}^*$ , (b,f,j) the RLS was assumed to be Reaction 2,  $\text{OH}^* \rightarrow \text{O}^*$ , (c,g,k) the RLS was assumed to be Reaction 3,  $\text{O}^* \rightarrow \text{OOH}^*$ , and for (d,h,l) the RLS was assumed to be Reaction 4,  $\text{OOH}^* \rightarrow * + \text{O}_2$ .

**Table S3: Quasi-equilibrium with phase-change reaction microkinetic modeling standard rate constants,  $k_i^0$ , symmetry coefficients,  $\theta_i$ , phase change voltages,  $E_{PhaseChange}^0$ , with 95% Confidence Intervals and RMS Log Error for fits of each possible rate limiting step on the DFT self-consistent  $\text{CoO}_x(\text{OH})_{2-x}$  ( $11\bar{2}0$ ) surfaces.  $E_{PhaseChange}^0 < 1.5\text{V vs. RHE}$  or  $> 1.9\text{V vs. RHE}$  are indicated as the lack of experimental data in this range prevented an accurate fit. These scenarios are considered to adopt the single phase noted in the table, i.e. the  $\beta\text{-Co}(\text{OH})_2$  surface concentration decreases at  $E > E_{PhaseChange}^0$  and  $\beta\text{-CoOOH}$  and  $\text{CoO}_2$  increase at  $E > E_{PhaseChange}^0$ .**

Phase:	Surface:	DFT Coverage Conditions:	RLS	$k_i^0$ ( $\text{s}^{-1}$ )	$\theta_i$	$E_{PhaseChange}^0$ ( $\text{V}_{\text{RHE}}$ )	RMS Log Error
$\beta\text{-Co}(\text{OH})_2$	$(11\bar{2}0)$	1 ML $\text{OH}^*$	$* \rightarrow \text{OH}^*$	$(2.1 \pm 0.3) \times 10^{-3}$	$0.35 \pm 0.02$	$> 1.9$	2.41
			$\text{OH}^* \rightarrow \text{O}^*$	$(2.3 \pm 0.6) \times 10^3$	$0.24 \pm 0.02$	$1.772 \pm 0.008$	2.26
			$\text{O}^* \rightarrow \text{OOH}^*$	$(6.0 \pm 0.5) \times 10^3$	$0.50 \pm 0.02$	$1.592 \pm 0.004$	1.83
			$\text{OOH}^* \rightarrow * + \text{O}_2$	$0.5 \pm 1.2$	$0.50 \pm 0.05$	$0.9993 \pm 0.0006$	7.20
$\beta\text{-CoOOH}$	$(11\bar{2}0)$	$\frac{1}{2}$ ML $\text{H}_2\text{O}^*$ $\frac{1}{2}$ ML $\text{OH}^*$	$* \rightarrow \text{OH}^*$	$(5 \pm 2) \times 10^{-5}$	$0.51 \pm 0.02$	$1.593 \pm 0.004$	1.16
			$\text{OH}^* \rightarrow \text{O}^*$	$(1.5 \pm 0.3) \times 10^3$	$0.51 \pm 0.02$	$1.593 \pm 0.004$	1.16
			$\text{O}^* \rightarrow \text{OOH}^*$	$(1 \pm 2) \times 10^6$	$1.00 \pm 0.05$	$< 1.5$	6.54
			$\text{OOH}^* \rightarrow * + \text{O}_2$	$10 \pm 18$	$1.00 \pm 0.05$	$1.70 \pm 0.01$	2.11
$\text{CoO}_2$	$(11\bar{2}0)$	$\frac{1}{2}$ ML $\text{H}_2\text{O}^*$ $\frac{1}{2}$ ML $\text{OH}^*$	$* \rightarrow \text{OH}^*$	$4.9 \pm 0.2$	$0.51 \pm 0.02$	$1.593 \pm 0.004$	1.16
			$\text{OH}^* \rightarrow \text{O}^*$	$22 \pm 8$	$1.00 \pm 0.02$	$< 1.5$	1.30
			$\text{O}^* \rightarrow \text{OOH}^*$	$(2 \pm 15) \times 10^9$	$1.0 \pm 0.2$	$< 1.5$	19.6
			$\text{OOH}^* \rightarrow * + \text{O}_2$	$(8 \pm 3) \times 10^{-8}$	$0.35 \pm 0.02$	$< 1.5$	2.41

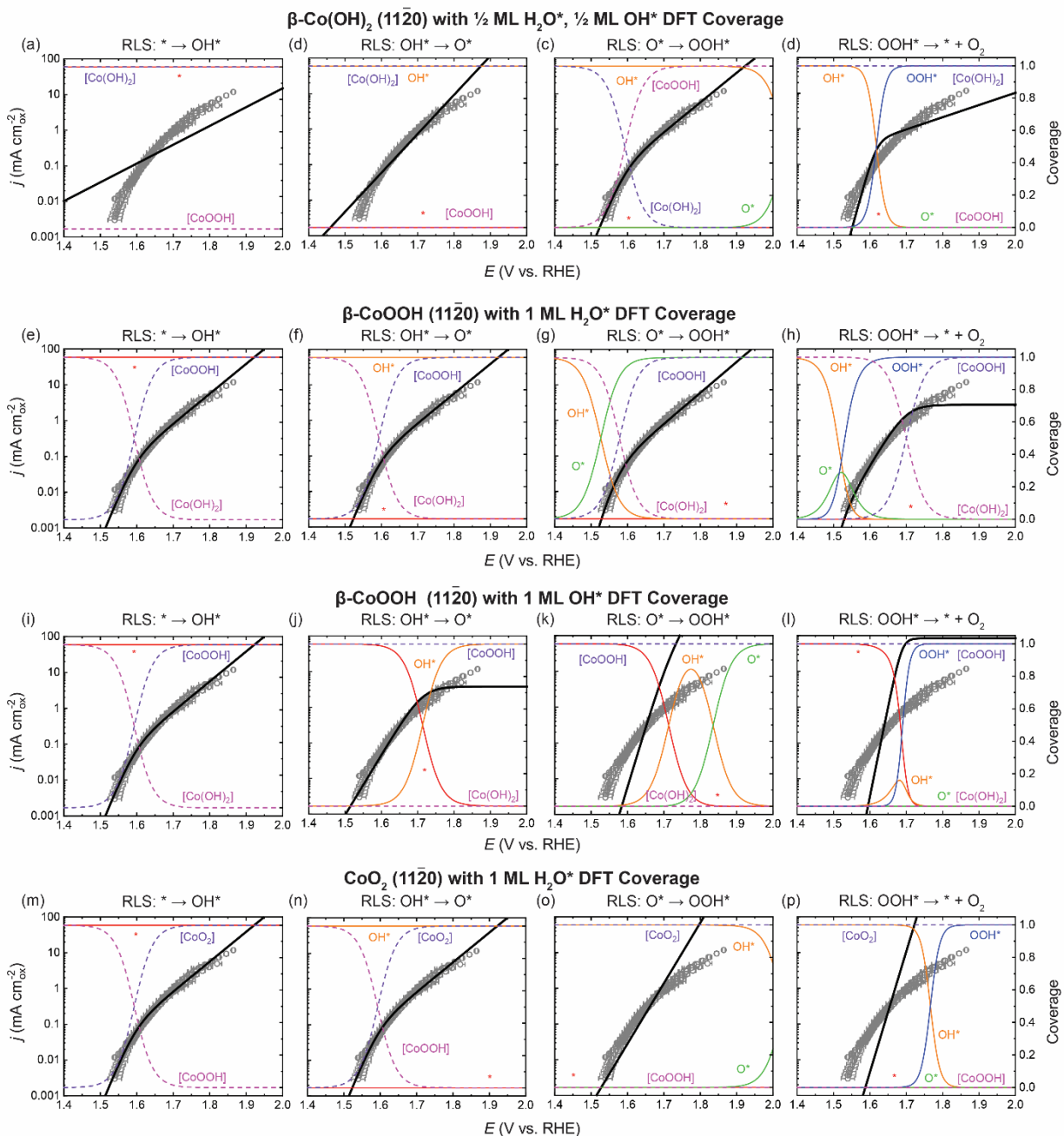


**Figure S5. Quasi-equilibrium with phase-change reaction microkinetic fits for the DFT non-self-consistent CoO<sub>x</sub>(OH)<sub>2-x</sub> (11 $\bar{2}$ 0) surfaces.** The fits are shown in black and the coverage predicted by the quasi-equilibrium microkinetic model shown in red for the clean surface, orange for OH\*, green for O\*, and blue for OOH\*, purple for the active phase, and magenta for the inactive phase for the (a-d)  $\beta$ -Co(OH)<sub>2</sub> (11 $\bar{2}$ 0) surface with ½ ML H<sub>2</sub>O\*, ½ ML OH\* DFT coverage, (e-h)  $\beta$ -CoOOH (11 $\bar{2}$ 0) surface with 1 ML H<sub>2</sub>O\* DFT coverage, (i-l)  $\beta$ -CoOOH (11 $\bar{2}$ 0) surface with 1 ML OH\* DFT coverage, and (m-p) the CoO<sub>2</sub> (11 $\bar{2}$ 0) surface with 1 ML H<sub>2</sub>O\* DFT coverage. For (a,e,i,m) the RLS was assumed to be Reaction 1, \*  $\rightarrow$  OH\*, (b,f,j,n) the RLS was assumed to be Reaction 2, OH\*  $\rightarrow$  O\*, (c,g,k,o) the RLS was assumed to be Reaction 3, O\*  $\rightarrow$  OOH\*, and for (d,h,l,p) the RLS was assumed to be Reaction 4, OOH\*  $\rightarrow$  \* + O<sub>2</sub>.

**Table S4: Quasi-equilibrium microkinetic modeling standard rate constants,  $k_i^0$ , symmetry coefficients,  $\theta_i$ , phase change voltages,  $E_{PhaseChange}^0$ , with 95% Confidence Intervals and RMS Log Error for fits of each possible rate limiting step on the DFT non-self-consistent  $\text{CoO}_x(\text{OH})_{2-x}$  (11 $\bar{2}$ 0) surfaces.  $E_{PhaseChange}^0 < 1.5\text{V vs. RHE}$  or  $> 1.9\text{V vs. RHE}$  are indicated as such and could not be fit accurately due to lack of experimental data. These scenarios are considered to adopt the single phase noted in the table.**

Phase:	Surface:	DFT Coverage Conditions:	RLS	$k_i^0$ ( $\text{s}^{-1}$ )	$\theta_i$	$E_{PhaseChange}^0$ ( $\text{V}_{\text{RHE}}$ )	RMS Log Error
$\beta$ -Co(OH) <sub>2</sub>	(11 $\bar{2}$ 0)	½ ML H <sub>2</sub> O* ½ ML OH*	* → OH*	$(4 \pm 23) \times 10^{-9}$	$0.69 \pm 0.05$	> 1.9	6.34
			OH* → O*	$(1.4 \pm 0.3) \times 10^4$	$0.35 \pm 0.02$	> 1.9	2.40
			O* → OOH*	$(7 \pm 1) \times 10^3$	$0.51 \pm 0.02$	$1.593 \pm 0.004$	1.16
			OOH* → * + O <sub>2</sub>	$2.0 \pm 0.2$	$0.80 \pm 0.03$	> 1.9	4.99
$\beta$ -CoOOH	(11 $\bar{2}$ 0)	1 ML H <sub>2</sub> O*	* → OH*	$(4.2 \pm 0.2) \times 10^{-5}$	$0.51 \pm 0.02$	$1.593 \pm 0.004$	1.16
			OH* → O*	$0.10 \pm 0.01$	$0.51 \pm 0.02$	$1.593 \pm 0.004$	1.16
			O* → OOH*	$(6.7 \pm 0.8) \times 10^{-2}$	$0.49 \pm 0.02$	$1.578 \pm 0.005$	1.25
			OOH* → * + O <sub>2</sub>	$9 \pm 19$	$1.00 \pm 0.05$	$1.70 \pm 0.01$	2.27
$\beta$ -CoOOH	(11 $\bar{2}$ 0)	1 ML OH*	* → OH*	$3.6 \pm 0.1$	$0.51 \pm 0.02$	$1.593 \pm 0.004$	1.16
			OH* → O*	$13 \pm 1$	$1.00 \pm 0.01$	< 1.5	2.24
			O* → OOH*	$(2 \pm 1) \times 10^4$	$1.0 \pm 0.1$	< 1.5	18.0
			OOH* → * + O <sub>2</sub>	$(3 \pm 30) \times 10^3$	$1.0 \pm 0.2$	< 1.5	23.1
CoO <sub>2</sub>	(11 $\bar{2}$ 0)	1 ML H <sub>2</sub> O*	* → OH*	$(8 \pm 4) \times 10^{-6}$	$0.51 \pm 0.02$	$1.593 \pm 0.004$	1.16
			OH* → O*	$(1.5 \pm 0.3) \times 10^2$	$0.51 \pm 0.02$	$1.593 \pm 0.004$	1.16
			O* → OOH*	$(1.7 \pm 0.6) \times 10^5$	$1.00 \pm 0.05$	< 1.5	6.54
			OOH* → * + O <sub>2</sub>	$(6 \pm 41) \times 10^3$	$1.0 \pm 0.1$	< 1.5	20.4

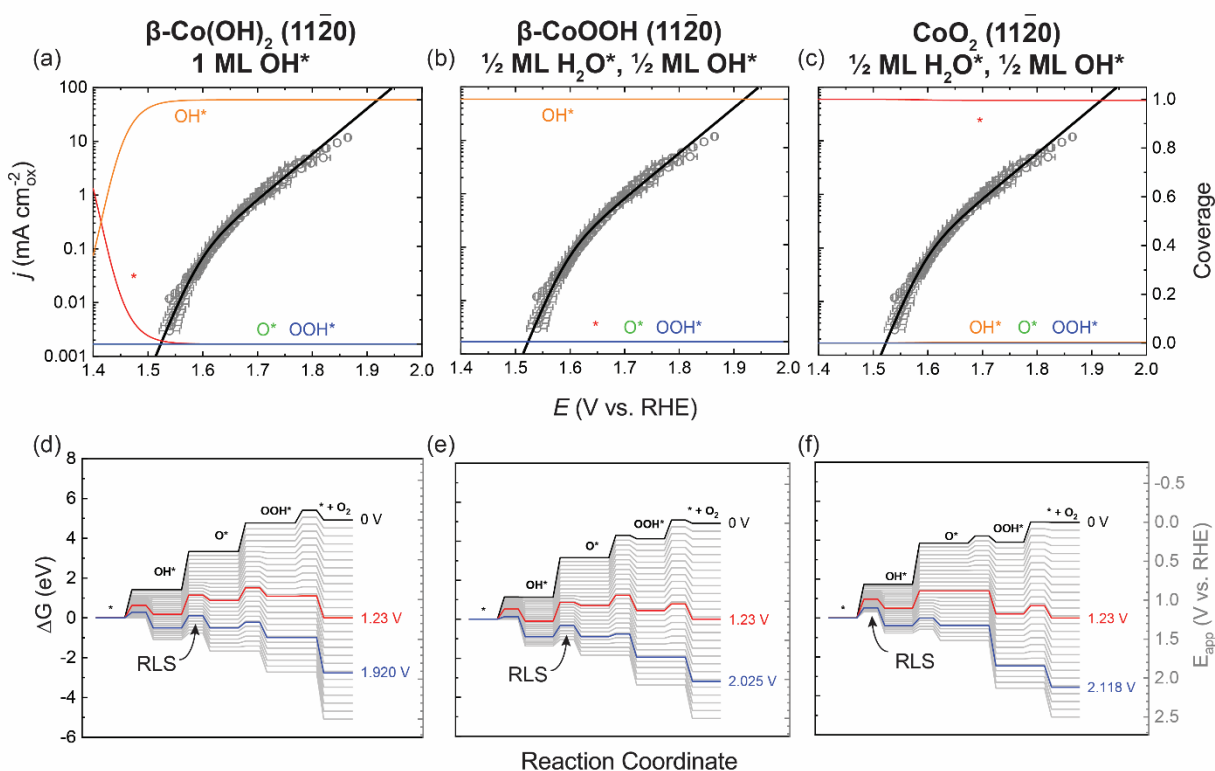


**Figure S6. Steady state microkinetic fits for the DFT self-consistent  $\text{CoO}_x(\text{OH})_{2-x} (11\bar{2}0)$  surfaces.** The fits are shown in black and the coverage predicted by the steady state microkinetic model shown in red for the clean surface, orange for  $\text{OH}^*$ , green for  $\text{O}^*$ , and blue for  $\text{OOH}^*$  for the (a)  $\beta\text{-Co}(\text{OH})_2 (11\bar{2}0)$  surface with 1 ML  $\text{OH}^*$  DFT coverage, (b)  $\beta\text{-CoOOH} (11\bar{2}0)$  surface with  $\frac{1}{2}$  ML  $\text{H}_2\text{O}^*$ ,  $\frac{1}{2}$  ML  $\text{OH}^*$  DFT coverage, and (c) the  $\text{CoO}_2 (11\bar{2}0)$  surface with  $\frac{1}{2}$  ML  $\text{H}_2\text{O}^*$ ,  $\frac{1}{2}$  ML  $\text{OH}^*$  DFT coverage. The full reaction coordinates at applied voltages from 0 to 2.5V vs. RHE in 0.1V increments are shown in (d) for the  $\beta\text{-Co}(\text{OH})_2 (11\bar{2}0)$  surface with 1 ML  $\text{OH}^*$  DFT coverage, (e) for the  $\beta\text{-CoOOH} (11\bar{2}0)$  surface with  $\frac{1}{2}$  ML  $\text{H}_2\text{O}^*$ ,  $\frac{1}{2}$  ML  $\text{OH}^*$  DFT coverage, and (f) for the  $\text{CoO}_2 (11\bar{2}0)$  surface with  $\frac{1}{2}$  ML  $\text{H}_2\text{O}^*$ ,  $\frac{1}{2}$  ML  $\text{OH}^*$  DFT coverage. The reaction coordinates at the standard OER potential ( $E^0 = 1.23\text{V}$  vs. RHE) and the PLS for the given bulk phase and surface are shown in red and blue, respectively.

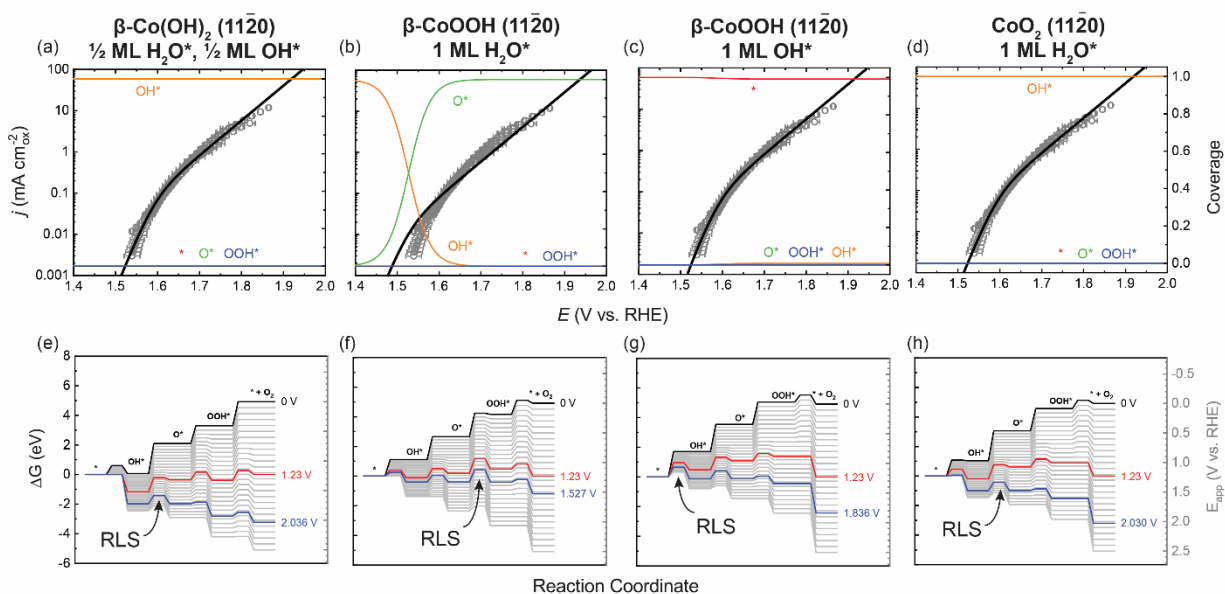


**Figure S7. Steady state microkinetic fits for the DFT non-self-consistent  $\text{CoO}_x(\text{OH})_{2-x} (11\bar{2}0)$ .** The fits are shown in black and the coverage predicted by the steady state microkinetic model shown in red for the clean surface, orange for  $\text{OH}^*$ , green for  $\text{O}^*$ , and blue for  $\text{OOH}^*$  for the (a)  $\beta\text{-Co}(\text{OH})_2 (11\bar{2}0)$  surface with  $\frac{1}{2}$  ML  $\text{H}_2\text{O}^*$ ,  $\frac{1}{2}$  ML  $\text{OH}^*$  DFT coverage, (b)  $\beta\text{-CoOOH} (11\bar{2}0)$  surface with 1 ML  $\text{H}_2\text{O}^*$  DFT coverage, (c)  $\beta\text{-CoOOH} (11\bar{2}0)$  surface with 1 ML  $\text{OH}^*$  DFT coverage, and (d) the  $\text{CoO}_2 (11\bar{2}0)$  surface with 1 ML  $\text{H}_2\text{O}^*$  DFT coverage. The full reaction coordinates at applied voltages from 0 to 2.5V vs. RHE in 0.1V increments are shown in (e) for the  $\beta\text{-Co}(\text{OH})_2 (11\bar{2}0)$  surface with  $\frac{1}{2}$  ML  $\text{H}_2\text{O}^*$ ,  $\frac{1}{2}$  ML  $\text{OH}^*$  DFT coverage, (f) for the  $\beta\text{-CoOOH} (11\bar{2}0)$  surface with 1 ML  $\text{H}_2\text{O}^*$  DFT coverage, (g) for the  $\beta\text{-CoOOH} (11\bar{2}0)$  surface with 1 ML  $\text{OH}^*$  DFT coverage, and (h) for the  $\text{CoO}_2 (11\bar{2}0)$  surface with 1 ML  $\text{H}_2\text{O}^*$  DFT coverage. The reaction coordinates at the standard OER potential ( $E^0 = 1.23\text{V}$  vs. RHE) and the PLS for the given bulk phase and surface are shown in red and blue, respectively.

Table S6: Steady State microkinetic modeling standard rate constants,  $k_i^0$ , with 95% Confidence Intervals and RMS Log Error for the fit on the DFT non-self-consistent  $\text{CoO}_x(\text{OH})_{2-x}$  ( $11\bar{2}0$ ) surfaces. The rate-limiting step is bolded.

Phase:	DFT Coverage Conditions:	Reaction Step	$k_i^0$ ( $\text{s}^{-1}$ )	$E_{i,DFT}^{0'}$ ( $\text{V}_{\text{RHE}}$ )	RMS Log Error
$\beta\text{-Co}(\text{OH})_2$	$\frac{1}{2}$ ML $\text{H}_2\text{O}^*$ $\frac{1}{2}$ ML $\text{OH}^*$	$* \rightarrow \text{OH}^*$	$1 \times 10^3 \pm 2 \times 10^9$	0.063	1.16
		<b><math>\text{OH}^* \rightarrow \text{O}^*</math></b>	<b><math>(2.29 \pm 0.07) \times 10^3</math></b>	<b>2.036</b>	
		$\text{O}^* \rightarrow \text{OOH}^*$	$(6.3 \pm 0.8) \times 10^2$	1.200	
		$\text{OOH}^* \rightarrow * + \text{O}_2$	$8 \times 10^4 \pm 4 \times 10^7$	1.617	
$\beta\text{-CoOOH}$	1 ML $\text{H}_2\text{O}^*$	$* \rightarrow \text{OH}^*$	$1 \times 10^5 \pm 2 \times 10^7$	1.123	1.16
		$\text{OH}^* \rightarrow \text{O}^*$	$1 \times 10^5 \pm 2 \times 10^7$	1.527	
		<b><math>\text{O}^* \rightarrow \text{OOH}^*</math></b>	<b><math>(5.5 \pm 0.4) \times 10^{-2}</math></b>	<b>1.516</b>	
		$\text{OOH}^* \rightarrow * + \text{O}_2$	$1 \times 10^3 \pm 4 \times 10^5$	0.751	
$\beta\text{-CoOOH}$	1 ML $\text{OH}^*$	<b><math>* \rightarrow \text{OH}^*</math></b>	<b><math>3.6 \pm 0.1</math></b>	<b>1.714</b>	1.18
		$\text{OH}^* \rightarrow \text{O}^*$	$(4.6 \pm 0.6) \times 10^3$	1.834	
		$\text{O}^* \rightarrow \text{OOH}^*$	$(1 \pm 3) \times 10^7$	1.513	
		$\text{OOH}^* \rightarrow * + \text{O}_2$	$2 \times 10^3 \pm 3 \times 10^9$	-0.145	
$\text{CoO}_2$	1 ML $\text{H}_2\text{O}^*$	$* \rightarrow \text{OH}^*$	$1 \times 10^3 \pm 3 \times 10^9$	1.041	1.16
		<b><math>\text{OH}^* \rightarrow \text{O}^*</math></b>	<b><math>(1.64 \pm 0.06) \times 10^3</math></b>	<b>2.030</b>	
		$\text{O}^* \rightarrow \text{OOH}^*$	$(1.5 \pm 0.1) \times 10^6$	1.503	
		$\text{OOH}^* \rightarrow * + \text{O}_2$	$1 \times 10^6 \pm 1 \times 10^{12}$	0.342	

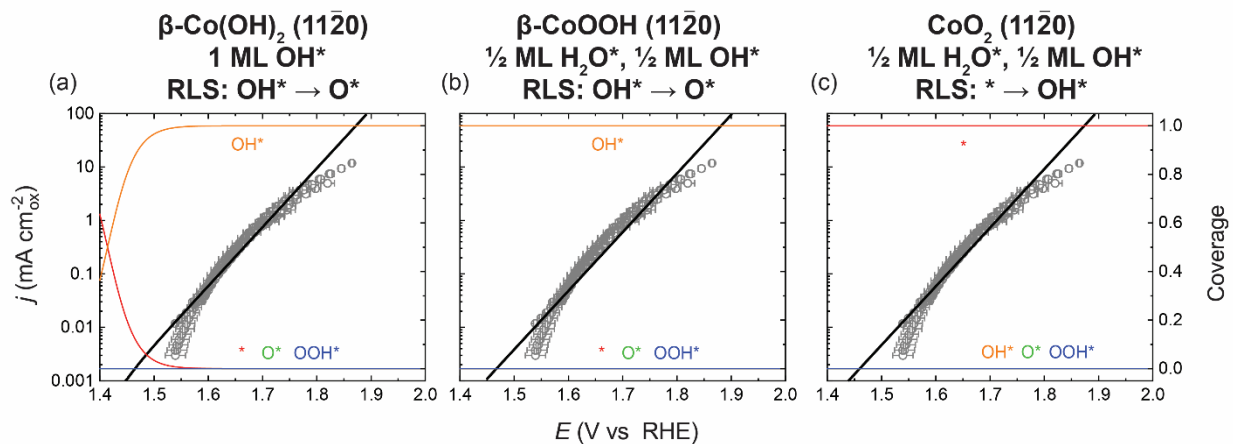


**Figure S8. Steady state microkinetic fits for the DFT self-consistent  $\text{CoO}_x(\text{OH})_{2-x}$  ( $11\bar{2}0$ ) surfaces assuming a single RLS dominates and no bulk phase-change reactions. (a-c) Show the single RLS steady state fit without the contribution of a bulk phase change reaction. The fits are shown in black and the coverage predicted by the steady state microkinetic model shown in red for the clean surface, orange for  $\text{OH}^*$ , green for  $\text{O}^*$ , and blue for  $\text{OOH}^*$  for the DFT self-consistent scenarios on the (a)  $\beta\text{-Co}(\text{OH})_2$  ( $11\bar{2}0$ ) surface with 1 ML  $\text{OH}^*$  coverage, (b) the  $\beta\text{-CoOOH}$  ( $11\bar{2}0$ ) surface with  $\frac{1}{2}$  ML  $\text{H}_2\text{O}^*$ ,  $\frac{1}{2}$  ML  $\text{OH}^*$  coverage, and (c) the  $\text{CoO}_2$  ( $11\bar{2}0$ ) surface with  $\frac{1}{2}$  ML  $\text{H}_2\text{O}^*$ ,  $\frac{1}{2}$  ML  $\text{OH}^*$  coverage.**

**Table S7: Steady state microkinetic modeling standard rate constants,  $k_i^0$ , symmetry coefficients,  $\theta_i$ , with 95% Confidence Intervals and RMS Log Error for fits assuming a single RLS dominates the reaction kinetics on the DFT self-consistent  $\text{CoO}_x(\text{OH})_{2-x}$  ( $11\bar{2}0$ ) surfaces.**

Phase:	DFT Coverage Conditions:	RLS	$k_{RLS}^0$ ( $\text{s}^{-1}$ )	$\theta_{RLS}$	RMS Log Error
$\beta\text{-Co}(\text{OH})_2$	1 ML $\text{OH}^*$	$\text{OH}^* \rightarrow \text{O}^*$	$796 \pm 3$	$0.348 \pm 0.003$	2.40
$\beta\text{-CoOOH}$	$\frac{1}{2}$ ML $\text{H}_2\text{O}^*$ $\frac{1}{2}$ ML $\text{OH}^*$	$\text{OH}^* \rightarrow \text{O}^*$	$(9.1 \pm 0.3) \times 10^3$	$0.351 \pm 0.003$	2.66
$\text{CoO}_2$	$\frac{1}{2}$ ML $\text{H}_2\text{O}^*$ $\frac{1}{2}$ ML $\text{OH}^*$	$* \rightarrow \text{OH}^*$	$5.3 \pm 0.1$	$0.35 \pm 0.01$	2.40

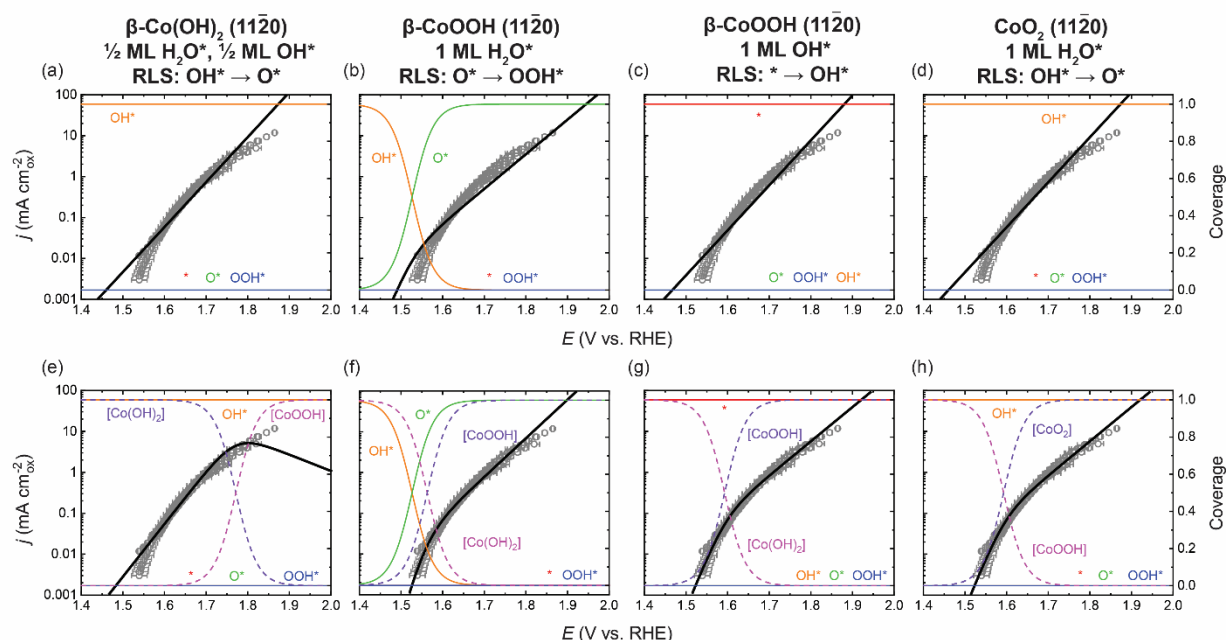


**Figure S9. Steady state microkinetic fits for the DFT non-self-consistent  $\text{CoO}_x(\text{OH})_{2-x}$  ( $11\bar{2}0$ ) surfaces assuming a single RLS dominates and contributions from bulk phase-change reactions.** The fits are shown in black and the coverage predicted are shown in red for the clean surface, orange for  $\text{OH}^*$ , green for  $\text{O}^*$ , and blue for  $\text{OOH}^*$ , purple for the active phase, and magenta for the inactive phase. (a-d) Show the single RLS steady state fit without the contribution of a bulk phase change reaction while (e-h) include the contribution of a bulk phase-change reaction. The DFT self-consistent fits are shown for the bulk phases with DFT simulated coverage conditions for the (a,d)  $\beta\text{-Co}(\text{OH})_2$  ( $11\bar{2}0$ ) surface with  $\frac{1}{2}$  ML  $\text{H}_2\text{O}^*$ ,  $\frac{1}{2}$  ML  $\text{OH}^*$  coverage, (b,f) the  $\beta\text{-CoOOH}$  ( $11\bar{2}0$ ) surface with 1 ML  $\text{H}_2\text{O}^*$  coverage, (c,g) the  $\beta\text{-CoOOH}$  ( $11\bar{2}0$ ) surface with 1 ML  $\text{OH}^*$  coverage, and (d,h) the  $\text{CoO}_2$  ( $11\bar{2}0$ ) surface with 1 ML  $\text{H}_2\text{O}^*$  coverage.

**Table S8: Steady state microkinetic modeling standard rate constants,  $k_{RLS}^0$ , symmetry coefficients,  $\theta_{RLS}$ , with 95% Confidence Intervals and RMS Log Error for fits assuming a single RLS dominates the reaction kinetics on the DFT non-self-consistent  $\text{CoO}_x(\text{OH})_{2-x}$  ( $11\bar{2}0$ ) surfaces.**

Phase:	DFT Coverage Conditions:	RLS	$k_i^0$ ( $\text{s}^{-1}$ )	$\theta_i$	RMS Log Error
$\beta\text{-Co}(\text{OH})_2$	$\frac{1}{2}$ ML $\text{H}_2\text{O}^*$ $\frac{1}{2}$ ML $\text{OH}^*$	$\text{OH}^* \rightarrow \text{O}^*$	$(1.4 \pm 0.4) \times 10^4$	$0.35 \pm 0.01$	2.40
$\beta\text{-CoOOH}$	1 ML $\text{H}_2\text{O}^*$	$\text{O}^* \rightarrow \text{OOH}^*$	$(5.5 \pm 0.1) \times 10^{-2}$	$0.50 \pm 0.01$	3.17
$\beta\text{-CoOOH}$	1 ML $\text{OH}^*$	$* \rightarrow \text{OH}^*$	$3.4 \pm 0.2$	$0.35 \pm 0.02$	2.71
$\text{CoO}_2$	1 ML $\text{H}_2\text{O}^*$	$\text{OH}^* \rightarrow \text{O}^*$	$(1.00 \pm 0.09) \times 10^4$	$0.350 \pm 0.007$	2.41

**Table S9: Steady state microkinetic modeling standard rate constants,  $k_{RLS}^0$ , symmetry coefficients,  $\theta_{RLS}$ , and phase change voltages,  $E_{\text{PhaseChange}}^0$ , with 95% Confidence Intervals and RMS Log Error for fits assuming a single RLS dominates the reaction kinetics and that the concentration of surface phase is voltage dependent on the DFT non-self-consistent  $\text{CoO}_x(\text{OH})_{2-x}$  ( $11\bar{2}0$ ) surfaces. These scenarios are considered to adopt the single phase noted in the table.**

Phase:	DFT Coverage Conditions:	RLS	$k_i^0$ ( $\text{s}^{-1}$ )	$\theta_i$	$E_{\text{PhaseChange}}^0$ ( $\text{V}_{\text{RHE}}$ )	RMS Log Error
$\beta\text{-Co}(\text{OH})_2$	$\frac{1}{2}$ ML $\text{H}_2\text{O}^*$ $\frac{1}{2}$ ML $\text{OH}^*$	$\text{OH}^* \rightarrow \text{O}^*$	$(8.8 \pm 0.3) \times 10^4$	$0.24 \pm 0.02$	$1.773 \pm 0.008$	1.76
$\beta\text{-CoOOH}$	1 ML $\text{H}_2\text{O}^*$	$\text{O}^* \rightarrow \text{OOH}^*$	$(5.600 \pm 0.001) \times 10^{-2}$	$0.440 \pm 0.001$	$1.563 \pm 0.005$	1.33
$\beta\text{-CoOOH}$	1 ML $\text{OH}^*$	$* \rightarrow \text{OH}^*$	$4.3 \pm 0.1$	$0.51 \pm 0.02$	$1.593 \pm 0.004$	1.16
$\text{CoO}_2$	1 ML $\text{H}_2\text{O}^*$	$\text{OH}^* \rightarrow \text{O}^*$	$(1.6 \pm 0.2) \times 10^3$	$0.505 \pm 0.008$	$1.593 \pm 0.003$	1.16

**Table S10: Bader charges  $q$  (in units of electrons) of Co active site and O-containing adsorbate and magnetic moment  $m$  (in units of  $\mu_B$ ) for Co active site on the different DFT non-self-consistent (11 $\bar{2}$ 0) surfaces of  $\text{CoO}_x(\text{OH})_{2-x}$ . Adsorbates involved in RLS are bolded.**

Phase:	Surface:	DFT Coverage Conditions:	Adsorbate	q:Co	q:O	m
Co(OH) <sub>2</sub>	(11 $\bar{2}$ 0)	½ ML H <sub>2</sub> O ½ ML OH*	*	1.21	-	2.68
			<b>OH*</b>	<b>1.37</b>	<b>-1.08</b>	<b>1.88</b>
			<b>O*</b>	<b>1.41</b>	<b>-0.66</b>	<b>2.12</b>
			OOH*	1.49	-1.02	1.94
CoOOH	(11 $\bar{2}$ 0)	1ML H <sub>2</sub> O*	*	1.44	-	1.95
			OH*	1.50	-1.53	1.90
			<b>O*</b>	<b>1.57</b>	<b>-0.73</b>	<b>2.15</b>
			<b>OOH*</b>	<b>1.60</b>	<b>-0.97</b>	<b>2.33</b>
CoOOH	(11 $\bar{2}$ 0)	1ML OH*	*	<b>1.48</b>	-	<b>2.22</b>
			<b>OH*</b>	<b>1.42</b>	<b>-1.05</b>	<b>0.65</b>
			O*	1.41	-0.34	0.68
			OOH*	1.35	-0.75	0.17
CoO <sub>2</sub>	(11 $\bar{2}$ 0)	1ML H <sub>2</sub> O*	*	1.52	-	0.91
			<b>OH*</b>	<b>1.61</b>	<b>-1.39</b>	<b>1.02</b>
			<b>O*</b>	<b>1.62</b>	<b>-0.53</b>	<b>1.18</b>
			OOH*	1.58	-0.89	0.90

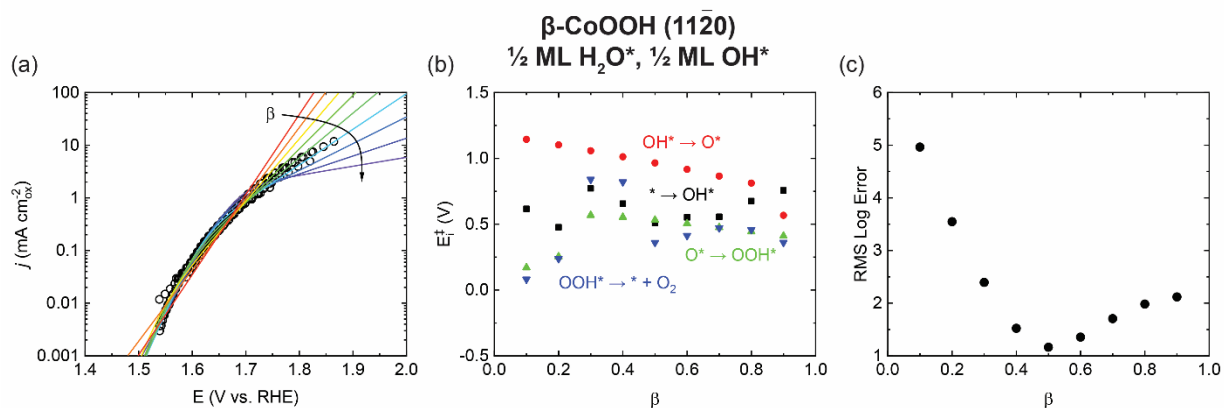


**Figure S10. Dependence of microkinetic model fit on choice of symmetry coefficient,  $\beta$ , in Step 5 for the  $\beta$ -CoOOH (11 $\bar{2}$ 0) surface with  $\frac{1}{2}$  ML H<sub>2</sub>O\*,  $\frac{1}{2}$  ML OH\* coverage.** (a) Microkinetic model fit as a function of  $\beta_i$  (where all  $\beta_i$  are equal to each other). (b) Reaction barrier height for each step as a function of  $\beta_i$ . (c) Goodness of fit as measured through the RMS log error as a function of  $\beta_i$ . As is shown the magnitude of the barrier height is a function of the symmetry coefficient, but the identity of the RLS remains step 2 ( $\text{OH}^* \rightarrow \text{O}^*$ ) for  $\beta$ -CoOOH outside of extreme value  $\beta_i > 0.9$ . The error is minimized at the fully symmetric  $\beta_i = 0.5$ .

**$\beta$ -CoOOH (11 $\bar{2}$ 0)**  
 $\frac{1}{2}$  ML H<sub>2</sub>O\*,  $\frac{1}{2}$  ML OH\*

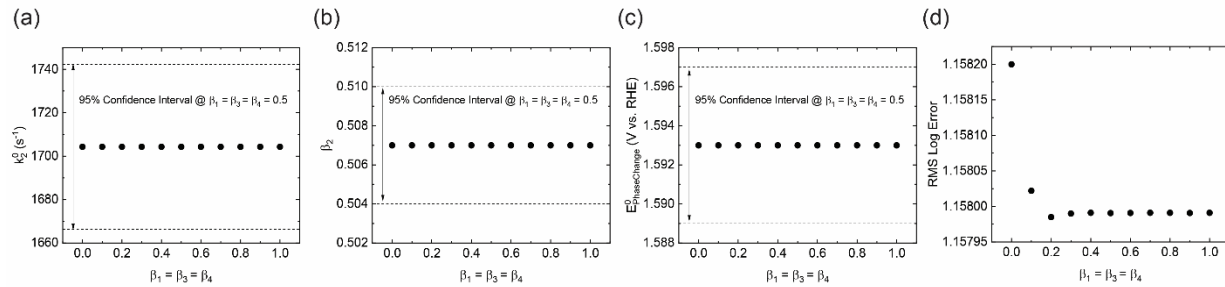


**Figure S11. Dependence of microkinetic model fit on choice of symmetry coefficient,  $\beta_i$ , in Step 7 for the  $\beta$ -CoOOH (11 $\bar{2}$ 0) surface with  $\frac{1}{2}$  ML H<sub>2</sub>O\*,  $\frac{1}{2}$  ML OH\*.** (a) Standard rate constants for the RLS ( $k^0_2$ ), (b) symmetry coefficient for the RLS ( $\beta_2$ ), (c) calculated phase change potential for each bulk phase ( $E^0_{\text{PhaseChange}}$ ), and (d) RMS log error as a function of the symmetry coefficients of the non-RLS steps (where  $\beta_1 = \beta_3 = \beta_4$ ). The results show that reactions (1), (3), and (4) are in quasi-equilibrium such that the choice of  $\beta$  has no influence on the values of the fitting parameters.

**Table S11: Adsorption energies ( $\Delta E$ ) published at Catalysis-hub.org repository under <https://www.catalysis-hub.org/publications/MeffordInterpreting2019>.<sup>11</sup> The gas DFT reference energies are for H<sub>2</sub>O and H<sub>2</sub> are -14.23092 and -6.77149 eV, respectively.**

Phase:	Surface:	DFT Coverage Conditions:	Adsorbate	$\Delta H$ [eV]
Co(OH) <sub>2</sub>	(11 $\bar{2}$ 0)	$\frac{1}{2}$ ML H <sub>2</sub> O* $\frac{1}{2}$ ML OH*	OH*	-0.23879
			O*	2.11361
			OOH*	2.95405
Co(OH) <sub>2</sub>	(11 $\bar{2}$ 0)	1 ML OH*	OH*	1.11227
			O*	3.34859
			OOH*	4.43025
CoOOH	(11 $\bar{2}$ 0)	1 ML H <sub>2</sub> O*	OH*	0.82111
			O*	2.66412
			OOH*	3.82051
CoOOH	(11 $\bar{2}$ 0)	$\frac{1}{2}$ ML H <sub>2</sub> O* $\frac{1}{2}$ ML OH*	OH*	0.82889
			O*	3.17036
			OOH*	3.78587
CoOOH	(11 $\bar{2}$ 0)	1 ML OH*	OH*	1.41142
			O*	3.56342
			OOH*	4.71673
CoO <sub>2</sub>	(11 $\bar{2}$ 0)	1 ML H <sub>2</sub> O*	OH*	0.73889
			O*	3.08536
			OOH*	4.22878
CoO <sub>2</sub>	(11 $\bar{2}$ 0)	$\frac{1}{2}$ ML H <sub>2</sub> O* $\frac{1}{2}$ ML OH*	OH*	1.43000
			O*	3.86448
			OOH*	3.55193

**Table S12: Vibrational and free-energy corrections  $\Delta G$  for H<sub>2</sub>O and H<sub>2</sub> gas and adsorbed OER intermediates needed to be added to  $\Delta E$  values in Table S11. For co-adsorbed water, only the entropy effects were considered, which is a good approximation for weakly adsorbed H<sub>2</sub>O.**

Molecule	ZPE [eV]	$\Delta CV$ [eV]	T $\Delta S$ (T=298 K) [eV]	$\Delta G(\text{gas})=ZPE+ \Delta CV- T\Delta S$ [eV]
H <sub>2</sub> O(g)	0.560	0.103	0.675 (at P = 0.035 bar)	-0.012
H <sub>2</sub> (g)	0.268	0.0905	0.408(at P = 1 bar)	-0.049
Adsorbate	ZPE [eV]	$\Delta CV$ [eV]	T $\Delta S$ (T=298 K) [eV]	$\Delta G=ZPE+ \Delta CV- T\Delta S - \Delta G(\text{gas})$ [eV]
OH*	0.344	0.051	0.080	0.3022
O*	0.065	0.038	0.080	-0.0145
OOH*	0.443	0.068	0.116	0.3447
H <sub>2</sub> O*	same as H <sub>2</sub> O(g)	same as H <sub>2</sub> O(g)	0	0.675

### Supplemental References:

- 1 T. Shinagawa, A. T. Garcia-Esparza and K. Takanabe, *Scientific Reports*, 2015, **5**, 13801.
- 2 J. O. Bockris, *J. Chem. Phys.*, 1956, **24**, 817–827.
- 3 A. Damjanovic, A. Dey and J. O. Bockris, *Electrochimica Acta*, 1966, **11**, 791–814.
- 4 M. E. G. Lyons and M. P. Brandon, *Journal of Electroanalytical Chemistry*, 2010, **641**, 119–130.
- 5 A. Bergmann, D. Teschner, E. Martinez-Moreno, H. Dau, J. F. de Araújo, M. Gliech, P. Strasser, P. Chernev and T. Reier, *Nature Communications*, 2015, **6**, 8625.
- 6 A. Bergmann, T. E. Jones, E. M. Moreno, D. Teschner, P. Chernev, M. Gliech, T. Reier, H. Dau and P. Strasser, *Nature Catalysis*, 2018, **1**, 711–719.
- 7 D. A. García-Osorio, R. Jaimes, J. Vazquez-Arenas, R. H. Lara and J. Alvarez-Ramirez, *J. Electrochem. Soc.*, 2017, **164**, E3321–E3328.
- 8 A. J. Bard and L. R. Faulkner, *Electrochemical Methods: Fundamentals and Applications*, John Wiley & Sons, Inc., New York, 2nd edn., 2001.
- 9 J. T. Mefford, A. R. Akbashev, L. Zhang and W. C. Chueh, *J. Phys. Chem. C*, , DOI:10.1021/acs.jpcc.9b03589.
- 10 L. Zhang, L. Sun, Z. Guan, S. Lee, Y. Li, H. D. Deng, Y. Li, N. L. Ahlborg, M. Boloor, N. A. Melosh and W. C. Chueh, *Nano Lett.*, 2017, **17**, 5264–5272.
- 11 K. T. Winther, M. J. Hoffmann, J. R. Boes, O. Mamun, M. Bajdich and T. Bligaard, *Sci Data*, 2019, **6**, 1–10.